J|A|C|S

A R T I C L E S

Comparison between the Geometric and Electronic Structures and Reactivities of {FeNO}^{7} and {FeO$_2$}^{8} Complexes: A Density Functional Theory Study

Gerhard Schenk, Monita Y. M. Pau, and Edward I. Solomon*

Contribution from the Department of Chemistry, Stanford University, Stanford, California 94305-5080

Received June 16, 2003; E-mail: edward.solomon@stanford.edu

Abstract: In a previous study, we analyzed the electronic structure of $S = \frac{3}{2}$ {FeNO}^{7} model complexes [Brown et al. *J. Am. Chem. Soc.* **1995**, *117*, 715−732]. The combined spectroscopic data and SCF-Xα-SW electronic structure calculations are best described in terms of Fe^{III} ($S = \frac{5}{2}$) antiferromagnetically coupled to NO$^-$ ($S = 1$). Many nitrosyl derivatives of non-heme iron enzymes have spectroscopic properties similar to those of these model complexes. These NO derivatives can serve as stable analogues of highly labile oxygen intermediates. It is thus essential to establish a reliable density functional theory (DFT) methodology for the geometry and energetics of {FeNO}^{7} complexes, based on detailed experimental data. This methodology can then be extended to the study of {FeO$_2$}^{8} complexes, followed by investigations into the reaction mechanisms of non-heme iron enzymes. Here, we have used the model complex Fe-(Me$_3$TACN)(NO)(N$_3$)$_2$ as an experimental marker and determined that a pure density functional BP86 with 10% hybrid character and a mixed triple-ζ/double-ζ basis set lead to agreement between experimental and computational data. This methodology is then applied to optimize the hypothetical Fe(Me$_3$TACN)(O$_2$)-(N$_3$)$_2$ complex, where the NO moiety is replaced by O$_2$. The main geometric differences are an elongated Fe−O$_2$ bond and a steeper Fe−O−O angle in the {FeO$_2$}^{8} complex. The electronic structure of {FeO$_2$}^{8} corresponds to Fe^{III} ($S = \frac{5}{2}$) antiferromagnetically coupled to O$_2^-$ ($S = \frac{1}{2}$), and, consistent with the extended bond length, the {FeO$_2$}^{8} unit has only one Fe^{III}−O$_2^-$ bonding interaction, while the {FeNO}^{7} unit has both σ and π type Fe^{III}−NO$^-$ bonds. This is in agreement with experiment as NO forms a more stable Fe^{III}−NO$^-$ adduct relative to O$_2^-$. Although NO is, in fact, harder to reduce, the resultant NO$^-$ species forms a more stable bond to Fe^{III} relative to O$_2^-$ due to the different bonding interactions.

Introduction

Mononuclear non-heme iron centers are present in a wide range of enzymes that carry out a multitude of biological processes involving O$_2$. These enzymes include lipoxygenases, the pterin-dependent phenylalanine hydroxylase, intra- and extradiol dioxygenases, α-ketoglutarate-dependent and related enzymes (e.g., clavaminate synthase, isopenicillin *N*-synthase), and Rieske-type dioxygenases.[1] The enzymatic reactions between O$_2$ and organic substrates are catalyzed either by a high-spin Fe^{2+} site, which is involved in O$_2$ activation, or by a high-spin Fe^{III} site, which activates substrates.

To understand the differences in reactivity of mononuclear non-heme iron enzymes, oxygen adducts have to be examined. However, due to their inherent instability, oxygen intermediates have been very difficult to study. In the absence of experimental data, NO has been used to mimic the activation of O$_2$ for catalysis. It is well established that NO reacts readily with various ferrous non-heme iron enzymes[2,3] and model com-

plexes[4−6] to form stable compounds. Often NO is used in the study of ferrous systems to render these otherwise EPR silent paramagnetic complexes. Many model complexes and most protein systems studied to date have a ground state with $S = \frac{3}{2}$ and are, according to the Enemark and Feltham notation,[7] of the {FeNO}^{7} type (7 is the sum of six Fe 3d and one NO π* valence electrons). Previously, two representative model complexes, FeEDTA−NO and Fe[Me$_3$TACN](NO)−(N$_3$)$_2$ (Figure 1, left; designated by **1**),[4] were singled out for a detailed investigation of their electronic structures.[5] From combined magnetochemical, EPR, magnetic circular dichroism, absorption, resonance Raman, and X-ray absorption data, accompanied by SCF-Xα-SW electronic structure calculations, it was concluded that the electronic structure of {FeNO}^{7} is best described as an antiferromagnetically coupled Fe^{III}($S = \frac{5}{2}$) − NO$^-$($S = 1$) complex. More recently, the observed isomer shifts in the

(1) Solomon, E. I.; Brunold, T. C.; Davis, M. I.; Kemsley, J. N.; Lee, S. K.; Lehnert, N.; Neese, F.; Skulan, A. J.; Yang, Y.-S.; Zhou, J. *Chem. Rev.* **2000**, *100*, 235−349.
(2) Arciero, D. M.; Orville, A. M.; Lipscomb, J. D. *J. Biol. Chem.* **1985**, *260*, 14035−14044.
(3) Chen, V. J.; Orville, A. M.; Harpel, M. R.; Frolik, C. A.; Surerus, K. K.; Munck, E.; Lipscomb, J. D. *J. Biol. Chem.* **1989**, *264*, 21677−21681.
(4) Pohl, K.; Wieghardt, K.; Nuber, B.; Weiss, J. *J. Chem. Soc., Dalton Trans.* **1987**, *1*, 187−192.
(5) Brown, C. A.; Pavlosky, M. A.; Westre, T. E.; Zhang, Y.; Hedman, B.; Hodgson, K. O.; Solomon, E. I. *J. Am. Chem. Soc.* **1995**, *117*, 715−732.
(6) Ray, M.; Golombek, A. P.; Hendrich, M. P.; Yap, G. P. A.; Liable-Sands, L. M.; Rheingold, A. L.; Borovik, A. S. *Inorg. Chem.* **1999**, *38*, 3110−3115.
(7) Enemark, J. H.; Feltham, R. D. *Coord. Chem. Rev.* **1974**, *13*, 339.
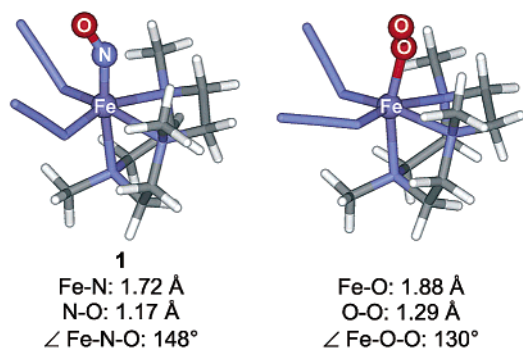
1

Fe-N: 1.72 Å
N-O: 1.17 Å
∠ Fe-N-O: 148°

Fe-O: 1.88 Å
O-O: 1.29 Å
∠ Fe-O-O: 130°

Figure 1. Structures of the geometry optimized {FeNO}[7] and {FeO$_2$}[8] model complexes. Starting from the crystal structure of **1**,[4] {FeNO}[7] was optimized using the hybrid functional BP86 + 10% HFX and the mixed basis set 6-311G*/6-31G*. {FeO$_2$}[8] was optimized similarly, after the NO ligand in **1** was replaced by O$_2$. Ligands other than NO or O$_2$ are presented in similar orientations for easy comparison of the Fe−NO and Fe−O$_2$ units.

Mössbauer spectrum of **1** were interpreted in terms of an octahedral species in an oxidation state lying between the ferric and ferrous forms.[8] However, a later analysis of the isomer shifts of a group of isostructural iron−nitrosyl complexes by Hauser et al. has demonstrated that Mössbauer spectroscopy is indeed a sensitive technique to assign oxidation states of iron in {FeNO}[6−8] complexes.[9] The result of their study is consistent with our earlier report[5] and supports the description of {FeNO}[7] as an antiferromagnetically coupled Fe^{III}($S = {}^5/_2$) − NO$^-$($S = 1$) complex. Furthermore, although the initial DFT calculations indicated that the electronic structure description of {FeNO}[7] may depend on the DFT method used, no effort has been undertaken to verify the selection of appropriate functionals or basis sets.[8] Because {FeNO}[7] serves as a model to study the electronic structure and reactivity of the closely related, reactive {FeO$_2$}[8] species (8 is the sum of six Fe 3d and two O$_2$ π^* valence electrons), it is essential to validate the appropriate level of theory by comparison to experimental data and extend it to the chemically relevant {FeO$_2$}[8] intermediate in O$_2$ activation.

Ab initio methods have found limited applicability in large systems, such as those of biological importance, due to slow convergence of the $3n$-dimensional wave function, where n is the number of electrons in the molecule. DFT is based on the Hohenberg−Kohn theorem[10] which allows one to express electronic energy, or any molecular property, as a functional of the electron density which only has three dimensions. Hence, DFT calculations[11] are more efficient and have become an important tool for the study of electronic structure and reactivity of bioinorganic systems,[12−14] which generally contain active sites composed of more than 40 atoms. Numerous functionals are now available, and it is an empirical process to select the most suitable one for the particular system under investigation. For instance, BP86,[15,16] one of the first gradient corrected DFT methods, often yields ground-state descriptions which are too

covalent. The introduction of hybrid functionals, developed to fit atomization and ionization energies as well as proton affinities of small organic molecules,[17,18] provides a means to adjust density functionals to reproduce experimentally observed data for a system of interest. Here, a broad range of density functionals and basis sets are applied to establish an optimal electronic structure description for **1**. This system has been chosen because the abundance of experimental data (vide supra) allows an accurate assessment of the performance of the various levels of theory. The optimized methodology is then applied to geometry optimize the {FeO$_2$}[8] oxygen analogue of **1** (Figure 1 right), and the geometries, bonding energetics, and electronic structures of the two complexes are compared. The outcome of the study provides insight into the activation of O$_2$ by a ferrous center and establishes the computational framework for the study of highly reactive, short-lived oxygen intermediates in mononuclear non-heme iron enzymes.

Methods

All geometry optimizations, unless otherwise indicated, were carried out spin-unrestricted, under stringent convergence criteria with the Gaussian 98 software package[19] starting from the crystal structure of **1**.[4] Both pure and hybrid functionals were utilized, and the adjustment of the amount and type of Hartree−Fock exchange (HFX) and correlation (DFC) was achieved using the IOp keywords of the Gaussian 98 program. The options 47 and 45 of Overlay 5 were utilized to construct the density functionals from local and nonlocal DF correlation and HFX, respectively. In this study, the Slater-type local density approximation[10,20,21] was used, supplemented with the Becke 1988 gradient corrected (GGA) functional (B88)[16] to define the total DF exchange. The Perdew 1986 (P86)[15] and Lee−Yang−Parr (LYP) nonlocal DF correlations[22,23] were employed with Perdew 1981 (P81)[24] and Vosko−Wilk−Nussair (VWN)[25] local correlation functionals, respectively. Among the well-defined hybrid functionals, Becke's three-parameter[26] with LYP (B3LYP) and P86 (BP86) correlation functionals and Becke's Half-and-Half exchange mixing[27] with LYP correlation (BHandHLYP) functionals were utilized. It should be noted that the default Gaussian 98 implementation of the BHandHLYP method does not correspond to the original definition by Becke because the HF exchange replaces only the total DF exchange without modifying the DF correlation. The B3LYP method is notable, because this method lacks 28% of the nonlocal DF exchange (ΔE_XB88) and 19% of the

(8) Rodriguez, J. H.; Xia, Y.-M.; Debrunner, P. G. *J. Am. Chem. Soc.* **1999**, *121*, 7846−7863.
(9) Hauser, C.; Glaser, T.; Eckhard, B.; Weyhermüller, T.; Wieghardt, K. *J. Am. Chem. Soc.* **2000**, *122*, 4352−4365.
(10) Hohenberg, P.; Kohn, W. *Phys. Rev.* **1964**, *136*, B864−B871.
(11) Koch, W.; Holthausen, M. C. *A Chemist's Guide to Density Functional Theory*; Wiley-VCH: Weinheim, 2000.
(12) Siegbahn, P. E. M.; Blomberg, M. R. A. *Chem. Rev.* **2000**, *100*, 421−437.
(13) Eriksson, L. A. *Theoretical Biochemistry: Processes and Properties of Biological systems*; Elsevier: Amsterdam, 2001; Vol. 9.
(14) Friesner, R. A.; Dunietz, B. D. *Acc. Chem. Res.* **2001**, *34*, 351−358.
(15) Perdew, J. P. *Phys. Rev. B: Condens. Matter* **1986**, *33*, 8822−8824.
(16) Becke, A. D. *Phys. Rev. A: Gen. Phys.* **1988**, *38*, 3098−3100.

(17) Pople, J. A.; Head-Gordon, M.; Fox, D. J.; Raghavachari, K.; Curtiss, L. A. *J. Chem. Phys.* **1989**, *90*, 5622−5629.
(18) Curtiss, L. A.; Jones, C.; Trucks, G. W.; Raghavachari, K.; Pople, J. A. *J. Chem. Phys.* **1990**, *93*, 2537−2545.
(19) Frisch, M. J.; Trucks, G. W.; Schlegel, H. B.; Scuseria, G. E.; Robb, M. A.; Cheeseman, J. R.; Zakrzewski, V. G.; Montgomery, J. A. J.; Stratmann, R. E.; Burant, J. C.; Dapprich, S.; Millam, J. M.; Daniels, A. D.; Kudin, K. N.; Strain, M. C.; Farkas, O.; Tomasi, J.; Barone, V.; Cossi, M.; Cammi, R.; Mennucci, B.; Pomelli, C.; Adamo, C.; Clifford, S.; Ochterski, J.; Petersson, G. A.; Ayala, P. Y.; Cui, Q.; Morokuma, K.; Malick, D. K.; Rabuck, A. D.; Raghavachari, K.; Foresman, J. B.; Cioslowski, J.; Ortiz, J. V.; Stefanov, B. B.; Liu, G.; Liashenko, A.; Piskorz, P.; Komaromi, I.; Gomperts, R.; Martin, R. L.; Fox, D. J.; Keith, T.; Al-Laham, M. A.; Peng, C. Y.; Nanayakkara, A.; Gonzalez, C.; Challacombe, M.; Gill, P. M. W.; Johnson, B.; Chen, W.; Wong, M. W.; Andres, J. L.; Head-Gordon, M.; Replogle, E. S.; Pople, J. A. *Gaussian 98*, revision A.1; Gaussian, Inc.: Pittsburgh, PA, 1998.
(20) Kohn, W.; Sham, L. J. *Phys. Rev.* **1965**, *140*, A1133−A1138.
(21) Slater, J. C. *The Self-Consistent Field for Molecules and Solids. Quantum Theory*; McGraw-Hill: New York, 1974; Vol. 4.
(22) Lee, C.; Yang, W.; Parr, R. G. *Phys. Rev. B: Condens. Matter* **1988**, *37*, 785−789.
(23) Miehlich, B.; Savin, A.; Stoll, H.; Preuss, H. *Chem. Phys. Lett.* **1989**, *157*, 200−206.
(24) Perdew, J. P.; Zunger, A. *Phys. Rev. B: Condens. Matter* **1981**, *23*, 5048−5079.
(25) Vosko, S. H.; Wilk, L.; Nusair, M. *Can. J. Phys.* **1980**, *58*, 1200−1211.
(26) Becke, A. D. *J. Chem. Phys.* **1993**, *98*, 5648−5652.
(27) Becke, A. D. *J. Chem. Phys.* **1993**, *98*, 1372−1377.

nonlocal DF correlation (ΔE_CLYP) as a result of the empirical parametrization ($E_{XC} = E_{XC}$LSDA + 0.72ΔE_XB88 + 0.20E_XHF − 0.20E_XLSDA + 0.81ΔE_CLYP), and the HF exchange (E_XHF) replaces 20% of the local DF exchange (E_XLSDA) component. Optimized models were visualized with Molden, version 3.7.[28] Superposition of the different optimized models and the crystal structure of **1** was carried out using the MSI InsightII software package. The most appropriate level of theory was selected on the basis of the lowest root-mean-square deviation (rmsd) from the crystal structure.

Vibrational and thermodynamic data for the optimized structures in the gas phase were obtained from spin-unrestricted single point calculations under tight convergence criteria. For solvent calculations, the polarized continuum model (PCM)[29−32] was applied, using a dielectric constant ϵ of 24.55 for ethanol.

To correlate calculations to experimental excited-state data, time-dependent (TD) DFT calculations[33−35] were carried out for geometry optimized models in Gaussian 98; to cover the entire energy range of interest, 30 excitations were calculated. Excitation energies were also calculated with the ΔSCF-DFT method[36] in ADF2001.[37−39] This program does not provide an option to generate hybrid functionals. Hence, to find the best agreement between experimentally determined and calculated excitation energies, spin-unrestricted single point calculations for both **1** and the model optimized in Gaussian 98 (using BP86 +10% HFX and 6-311G*/6-31G* (vide infra)) were performed under tight convergence criteria using the ADF package, and the effective nuclear charge (Z_{eff}) was varied in small increments between 25.40 and 26.00. The ground-state wave functions were used as initial guesses to obtain excited-state wave functions, where charge was transferred from an occupied to an unoccupied orbital. Excitation energies were calculated as differences of total energies between excited and ground states (ΔSCF-DFT method).[36] Because it was not possible to converge excited-state wave functions directly by transferring one electron, partial charge was initially transferred, and the resulting wave function was used as a starting point for the next calculation. The change in total energy increases linearly with the partial charge transferred. In this manner, it was possible to determine the excitation energy through extrapolation of the change in energy with the partial charge transferred.

Orbital coefficients from Gaussian 98 outputs were subjected to both the Mulliken and the natural population analysis (NPA).[40,41] The relative contribution of atomic Gaussian-type orbitals (AOs) to molecular orbitals (MOs) was evaluated using the AOMix program.[42,43]

Two approaches were taken to determine the energetics of NO/O₂ bonding: (1) Starting from the crystal structure of **1**, the NO was removed, and the fictitious ferrous five-coordinate (5C) complex was geometry optimized using the same methodology established for the FeNO complex. The neutral ligands (NO and O₂) were optimized similarly. The bonding energy was determined from the following equation:
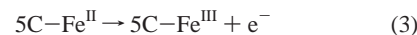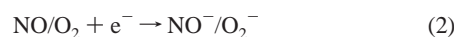
$$5C-Fe^{II} + NO/O_2 \rightarrow 6C-FeNO/O_2 \tag{1}$$

(28) Schaftenaar, G.; Noordik, J. H. *J. Comput.-Aided Mol. Des.* **2000**, *14*, 123−134.
(29) Pascual-Ahuir, J. L.; Silla, E.; Tomasi, J.; Bonaccorsi, R. *J. Comput. Chem.* **1987**, *8*, 778−787.
(30) Floris, F.; Tomasi, J. *J. Comput. Chem.* **1989**, *10*, 616−627.
(31) Cossi, M.; Barone, V.; Cammi, R.; Tomasi, J. *Chem. Phys. Lett.* **1996**, *255*, 327−335.
(32) Barone, V.; Cossi, M.; Tomasi, J. *J. Comput. Chem.* **1998**, *19*, 404−417.
(33) Casida, M. E. In *Recent Advances in Density Functional Theory*; Chong, D. P., Ed.; World Scientific: Singapore, 1995; Vol. 1, p 155.
(34) Gross, E. U. K. In *Density Functional Theory*; Nalewajski, R. F., Ed.; Springer: Heidelberg, 1996.
(35) Stratmann, R. E.; Scuseria, G. E.; Frisch, M. J. *J. Chem. Phys.* **1998**, *109*, 8218−8224.
(36) Ziegler, T.; Rauk, A.; Baerends, E. J. *Theor. Chim. Acta* **1977**, *43*, 261−271.
(37) Baerends, E. J.; Ellis, D. E.; Ros, P. *Chem. Phys.* **1973**, *2*, 41−51.
(38) Versluis, L.; Ziegler, T. *J. Chem. Phys.* **1988**, *88*, 322−328.
(39) Te Velde, G.; Baerends, E. J. *J. Comput. Phys.* **1992**, *99*, 84−98.

Table 1. Dependence of Geometric Parameters on the Level of Theory[a]

		geometric parameters				
		Fe₁–N₃₅	N₃₅–O₃₆	∠Fe₁–N₃₅–O₃₆	ΦFe–L[b]	rmsd (×1000)
	crystal structure	1.74 Å	1.14 Å	155°	2.17 Å	
1	BP86	1.73 Å	1.24 Å	149°	2.19 Å	64
2	BLYP	1.75 Å	1.24 Å	149°	2.23 Å	79
3	BP86; 10% HFX	1.78 Å	1.22 Å	144°	2.19 Å	56
4	BP86; 20% HFX	1.85 Å	1.23 Å	149°	2.18 Å	63
5	B3LYP	1.88 Å	1.23 Å	145°	2.20 Å	76
6	BHandHLYP	1.91 Å	1.23 Å	145°	2.16 Å	72
7	BHandHP86	1.94 Å	1.24 Å	144°	2.18 Å	82
8	BLYP; 20% HFX	1.89 Å	1.23 Å	144°	2.21 Å	79
9	BLYP; 80% DFC	1.77 Å	1.25 Å	150°	2.25 Å	89
10	BP86; 80% DFC	1.75 Å	1.24 Å	150°	2.22 Å	75
11	BP86; ADF {BSV}	1.70 Å	1.18 Å	151°	2.24 Å	127

[a] Optimizations 1−10 were carried out in Gaussian 98 using the double-ζ basis set LanL2DZ. Model 11 was optimized in ADF2001, using the triple-ζ basis set V. [b] Average distance of the five Fe−L bonds without NO.

(2) Alternatively, the 5C complex was optimized in the ferric oxidation state, and the ligands were optimized in their reduced states (NO⁻, O₂⁻). The optimized structures were subjected to single point calculations in solvent (ethanol), and the bonding interactions were then quantitated from the equations below:

$$NO/O_2 + e^- \rightarrow NO^-/O_2^- \tag{2}$$

$$5C-Fe^{II} \rightarrow 5C-Fe^{III} + e^- \tag{3}$$

$$5C-Fe^{III} + NO^-/O_2^- \rightarrow 6C-FeNO/O_2 \tag{4}$$

The bonding description was further analyzed by a comparison of the energy level diagrams and MOs for the {FeNO}[7] and {FeO₂}[8] complexes. MOs were generated both from Gaussian 98 and from ADF2001 outputs; because they are qualitatively very similar, only Gaussian orbitals (generated with Molden, version 3.7[28]) are presented here.

Results and Analysis

1. Functional Dependence. In this study, we use the crystal structure of **1** as an experimental marker; the complex was geometry optimized with a variety of functionals (vide supra). Starting with the pure density functionals BP86[15,16] and BLYP,[22] we varied the amount of HFX and total correlation. In each model, the basis set was the double-ζ LanL2DZ, which applies effective core potentials[44−46] to atoms in the third row and below. Table 1 lists the relevant geometric parameters and the rmsd values. In general, good agreement with the crystal structure is found, with the hybrid functional BP86 + 10% HFX performing best. However, for all models optimized with Gaussian 98, the experimental geometry of the FeNO unit is not well reproduced in the calculations (Table 1). In particular, the N−O bond length is overestimated by approximately 0.1 Å. A significantly better match to experimental data was achieved in the model optimized in ADF2001, using the pure BP86 functional together with the all-electron, triple-ζ basis set V (row 11 in Table 1). Comparison to the model optimized

(40) Mulliken, R. S. *J. Chem. Phys.* **1955**, *23*, 1833−1840.
(41) Reed, A. E.; Curtiss, L. A.; Weinhold, F. *Chem. Rev.* **1988**, *88*, 899−926.
(42) Gorelsky, S. I. AOMix program, revision 5.2.
(43) Gorelsky, S. I.; Lever, A. B. P. *J. Organomet. Chem.* **2001**, *635*, 187−196.
(44) Hay, P. J.; Wadt, W. R. *J. Chem. Phys.* **1985**, *82*, 270−283.
(45) Wadt, W. R.; Hay, P. J. *J. Chem. Phys.* **1985**, *82*, 284−298.
(46) Hay, P. J.; Wadt, W. R. *J. Chem. Phys.* **1985**, *82*, 299−310.

Table 2. Basis Set Effect on Geometries of NO^+, NO, and NO^- Using BP86 + 10% HFX

basis set	NO^+ (Å)	NO (Å)	NO^- (Å)
LanL2DZ	1.11	1.21	1.34
6-311G	1.09	1.19	1.33
6-311G*	1.06	1.15	1.28
6-311+G*	1.06	1.15	1.27
TZV	1.09	1.19	1.33
experimental	1.06[a]	1.15[b]	1.26[b]

[a] See ref 52. [b] See ref 53.

with the same functional in Gaussian 98 (row 2 in Table 1) strongly suggests that there is a significant effect due to the different basis sets used in these geometry optimizations. Hence, in addition to establishing a reasonable hybrid functional (BP86 + 10% HFX), we had to determine an appropriate basis set.

2. Basis Set Dependence. In an initial step, several basis sets were tested using NO^+, NO, and NO^- as markers for the geometry optimizations. In each case, the functional of choice was BP86 + 10% HFX. The results are summarized in Table 2. Models optimized with LanL2DZ[44−46] overestimate experimentally determined bond lengths by ∼0.05 Å. A slight improvement was achieved when triple-ζ basis sets (6-311G,[47,48] TZV[49]) instead of a double-ζ basis set were used. Addition of polarization functions to 6-311G (6-311G*) further improved the description of the bond lengths when compared to experiment. Incorporation of diffuse functions (6-311+G*) did not lead to significant improvements. The problem that arises is that 6-311G* is too large of a basis set to allow for geometry optimizations for large molecules on a practical time scale. Hence, a mixed basis set was introduced for the optimization of **1**, where the FeNO unit is described by the above triple-ζ basis set 6-311G* and the remainder of the complex by the analogous double-ζ basis set 6-31G*.[50,51] In Table 3, the effects of the purely triple-ζ basis set 6-311G* and the mixed triple- and double-ζ basis set 6-311G*/6-31G* on the geometry optimization of **1** are compared. Both basis sets lead to similar geometries, which are in good agreement with the experimentally determined parameters. The two commonly applied functionals BP86 and B3LYP have also been applied to optimize complex **1**, using the mixed basis set (Table 3). Consistent with the result from Table 1, these methodologies lead to greater deviations from the experimental geometry than the optimized functional BP86 + 10% HFX.

A closer look at the five Fe−L bond lengths (where L represents any ligand other than NO) indicates that the larger the basis set, the more the Fe−azide distances are underestimated, and the more the Fe−Me$_3$TACN distances are overestimated (see Tables 1 and 3). It is anticipated that in the gas phase the more extended basis sets will lead to better agreement with experimentally determined atomic distances. The deviation from this trend is due to the presence of both intra-

and intermolecular H-bond interactions in the solid state. To gain an estimate for the effect of these interactions on the model optimization, **1** was partially optimized with the five Fe−L distances fixed at the crystallographically determined values. The total energy of the partially optimized model complex increases by only 2.1 kcal/mol as compared to the fully optimized structure. Thus, crystal packing effects do not appear to affect optimizations significantly and are not further considered here.

3. Comparison to Spectroscopic Data. The accuracy of this geometrically established functional (BP86 + 10%HFX) and basis set (6-311G*/6-31G*) can be further evaluated by comparison to spectroscopic data for complex **1**. Here, we focus on two sets of physical parameters for comparison: the N−O stretch vibration and three $NO^- \rightarrow Fe^{III}$ charge transfer (CT) transitions.[5] Table 4 lists the experimental N−O stretch vibration[5] and the calculated values obtained from models optimized with BP86, BP86 + 10% HFX, and B3LYP, using 6-311G*/6-31G* as the basis set in all cases. N−O stretch vibrations calculated with BP86 and BP86 + 10% HFX both show reasonable and better agreement with resonance Raman data than that obtained from B3LYP. The pure density functional BP86 underestimated and BP86 + 10% HFX overestimated the experimental value, indicating that a slight reduction of HFX from 10% would give agreement with vibrational data.

Spectroscopic studies of **1**, including absorption (Abs), magnetic circular dichroism (MCD), and resonance Raman (rR), have revealed the presence of six transitions (Figure 2); the two low energy transitions (bands 1 and 2) are ascribed as formally forbidden ferric d → d ligand field (LF) transitions, which gain intensities through spin−orbit coupling to the $NO^- \rightarrow Fe^{III}$ CT transitions and through the exchange interaction between Fe^{III} ($S = ^5/_2$) and NO^- ($S = 1$).[5] The highest energy transition (band 6) in Figure 2 was assigned by resonance Raman as an $N_3^- \rightarrow Fe^{III}$ CT transition, while bands 3 to 5 are due to CT transitions from NO^- to Fe^{III}.[5] The Gaussian 98 software package offers the option to calculate transitions using time-dependent DFT (TDDFT). In Figure 2, the results for the FeNO model optimized with BP86 + 10% HFX and 6-311G*/6-31G* are illustrated. In each case, 30 excitations were calculated to cover the entire energy range of interest. None of the experimental transitions were reproduced by the calculations.[54] Because TDDFT leads to a poor representation of experimental data, we applied ΔSCF-DFT calculations in ADF2001 to determine the accuracy of the established methodology. Using the pure functional BP86 and the triple-ζ basis set V to obtain ground-state wave functions for the crystal structure gave only modest agreement with the experimental transitions ES1 − ES3 (calculated: 14 440, 17 870, 18 920 cm^{-1} vs experimental: 16 450, 18 440, 21 000 cm^{-1} respectively). However, the match could be improved by gradually lowering the Z_{eff} from 26.00 to 25.40. ΔSCF-DFT calculations were carried out for both the crystal structure and the model optimized in Gaussian 98 (using BP86 + 10% HFX with the mixed 6-311G*/6-31G* basis set). The results are summarized in Table 5 along with the experimental values. For both the crystal structure and the optimized model, similar excitation energies were calculated. Figure 3 shows a plot of

(47) McGrath, M. P.; Radom, L. *J. Chem. Phys.* **1991**, *94*, 511−516.
(48) Curtiss, L. A.; McGrath, M. P.; Blaudeau, J.-P.; Davis, N. E.; Binning, R. C. J.; Radom, L. *J. Chem. Phys.* **1995**, *103*, 6104−6113.
(49) Schaefer, A.; Huber, C.; Ahlrichs, R. *J. Chem. Phys.* **1994**, *100*, 5829−5835.
(50) Rassolov, V. A.; Pople, J. A.; Ratner, M. A.; Windus, T. L. *J. Chem. Phys.* **1998**, *109*, 1223−1229.
(51) Hehre, W. J.; Random, L.; Schleyer, P. v. R.; Pople, J. A. *Ab Initio Molecular Orbital Theory*; Wiley: New York, 1986.
(52) In *Tables of Interatomic Distances and Configuration in Molecules and Ions*; Sutton, L. E., Ed.; Chemical Society: London, 1958.
(53) Tronc, M.; Huetz, A.; Landau, M.; Pichou, F.; Reinhardt, J. *J. Phys. B* **1975**, *8*, 1160−1169.

(54) Similarly, poor agreement with experimental transitions is observed in TDDFT calculations for the FeNO model optimized with B3LYP and 6-311G*/6-31G* as shown in Figure S1.

Table 3. Comparison between 6-311G* and 6-311G*/6-31G* for **1** Optimized with BP86 + 10% HFX (Geometric Parameters for **1** Optimized with BP86 and B3LYP using the Mixed Basis Set are included)

geometric parameter	crystal structure	6-311G* BP86/10% HFX	6-311G*/6-31G* BP86/10% HFX	6-311G*/6-31G* BP86	6-311G*/6-31G* B3LYP
Fe−N (Å)	1.74	1.73	1.72	1.70	1.83
N−O (Å)	1.14	1.17	1.17	1.19	1.18
∠Fe−N−O (deg)	155	149	148	148	149
ΦFe−L (Å)[a]	2.17	2.20	2.19	2.19	2.20

[a] Average distance of the five Fe−L bonds without NO/O2.

Table 4. Experimental[a] and Calculated N−O Stretch Vibrations of Complex **1**, with 6-311G*/6-31G* in All Calculations

	N−O stretch vibration (cm^{-1})
BP86	1697
BP86 + 10% HFX	1758
B3LYP	1780
experimental[a]	1712

[a] See ref 5 for details.
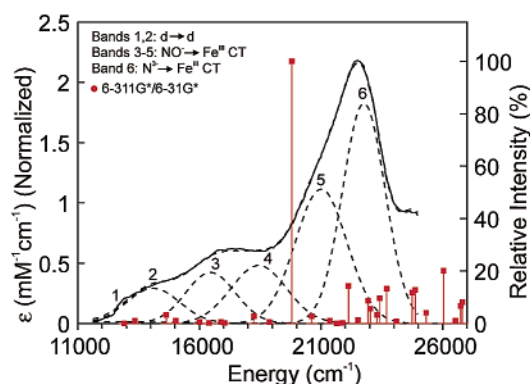
Figure 2. Low temperature (100 K) absorption spectrum of **1** (Reprinted from ref 5. Copyright 1995 American Chemical Society). The Gaussian resolved transitions are ascribed to Fe^{III} d → d transitions (bands 1 and 2), NO$^-$ → Fe^{III} CT transitions (bands 3−5), and the azide → Fe^{III} CT transition (N$_3^-$). TDDFT calculations on {FeNO}[7] optimized using BP86 + 10% HFX with 6-311G*/6-31G* (red).

Table 5. Experimental[a] and ΔSCF-DFT[b] Data for NO$^-$ → Fe^{III} CT Transitions in Complex **1**

	Gaussian optimized model			crystal structure		
Z_{eff}	ES1[c]	ES2[c]	ES3[c]	ES1[c]	ES2[c]	ES3[c]
25.40	16 570	20 280	20 690			
25.45	16 545	20 080	20 300			
25.50	16 245	19 940	20 190			
25.55	16 060	19 760	20 070	16 170	19 760	20 070
25.60	15 975	19 565	19 950	16 085	19 645	19 950
25.65	15 765	19 360	19 830	15 765	19 570	19 825
25.70	15 605	19 155	19 700	15 545	19 155	19 510
25.85	15 120	18 490	19 350	14 705	18 190	19 154
experimental[a]	16 450	18 440	21 000			

[a] See ref 5 for details. [b] All calculations done with ADF2001. [c] ES1, ES2, ES3 correspond to band 3, band 4, and band 5 in Figure 2, respectively; energies in cm^{-1}.

Z_{eff} versus the sum of the least squares of the deviations from experimental data, indicating a minimum at $Z_{eff} \approx 25.60$.[55]

It is crucial to compare the ground-state wave functions obtained in Gaussian 98 using BP86 + 10% HFX with

(55) For comparison, ΔSCF-DFT calculations with varied Z_{eff} were also carried out for the model optimized in Gaussian 98 using B3LYP with the mixed basis set. The ground-state wave function in ADF2001 was obtained using the pure density functionals BLYP and BP86 with the triple-ζ basis set V. The closest agreement between experiment and calculation was again reached at $Z_{eff} \approx 25.60$ (Table S1).
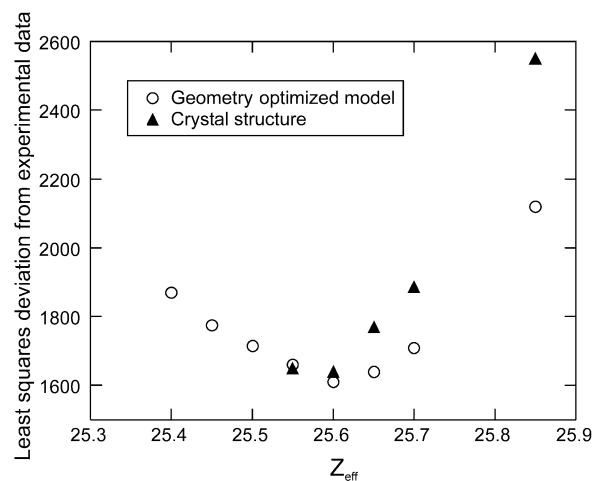
Figure 3. Correlation between experimental and calculated transitions using the ΔSCF-DFT method. Both the crystal structure of **1** and the {FeNO}[7] model optimized with BP86 + 10% HFX (using 6-311G*/6-31G*) were used for single point calculations in ADF2001. The Z_{eff} was altered stepwise, and the calculated transitions were compared to the experimental values using the least-squares approach.

ADF2001 using BP86 and modified Z_{eff}, because both methods should result in a similar electronic structure description. The two wave functions were compared on the basis of the calculated spin densities for the metal ion and NO, because spin density gives a measurement of covalency and thus the bonding description. The Gaussian optimized model with BP86 + 10% HFX has a Fe SD of 3.27 and a NO SD of −0.71, while the wave function of the optimized model obtained in ADF2001 using BP86 with the triple-ζ basis set V and Z_{eff} of 25.60 gives a Fe SD of 3.25 and a NO SD of −0.60. Consequently, both methods converge to very similar descriptions for the electronic structure of **1**.[56] In contrast, the model optimized with BP86 gives a too covalent (Fe SD, 2.75; NO SD, −0.29) and that with B3LYP gives a too ionic (Fe SD, 3.75; NO SD, −1.11) description of bonding.

4. Geometry Optimization of the {FeO2}[8] Model Complex. Starting from the crystal structure of **1**, the NO was replaced by O2, and the geometry of the resulting complex was optimized using the functional BP86 + 10% HFX. Both the double-ζ LanL2DZ and the mixed basis set 6-311G*/6-31G* were used. In principle, different spin states (S_{tot} = 1, 2, 3) are possible. However, S_{tot} = 2 is energetically favored, being 9.3 and 12.4 kcal/mol more stable than the S_{tot} =1 and S_{tot} = 3 states, respectively.[57] Furthermore, the S_{tot} = 3 state involves ferromag-

(56) Comparison of the spin densities obtained from ground-state wave functions in ADF2001 using the optimal Z_{eff} = 25.60 (Table S1) with two different functionals and two different structures shows that spin densities have a stronger dependence on geometry than the choice of functional (Table S2). This observation supports the choice of BP86 + 10% HFX, which gives the best geometric agreement to the crystal structure.

Table 6. Comparison of BP86 + 10% HFX Geometry Optimized NO and O_2 Models, Using LanL2DZ and 6-311G*/6-31G* as Basis Sets

geometric parameters	1	FeNO model		FeO$_2$ model	
		LanL2DZ	6-311G*/ 6-31G*	LanL2DZ	6-311G*/ 6-31G*
Fe$_1$–N$_{35}$	1.74 Å	1.78 Å	1.72 Å		
Fe$_1$–O$_{35}$				2.03 Å	1.88 Å
N$_{35}$–O$_{36}$	1.14 Å	1.22 Å	1.17 Å		
O$_{35}$–O$_{36}$				1.37 Å	1.29 Å
∠Fe$_1$–N$_{35}$–O$_{36}$	155°	144°	148°		
∠Fe$_1$–O$_{35}$–O$_{36}$				109°	130°
ΦFe$_1$–L^a	2.17 Å	2.19 Å	2.19 Å	2.18 Å	2.16 Å

^{a} Average distance of the five Fe–L bonds without NO/O$_2$.

netic coupling of the electrons of triplet O_2 with those on Fe, which is not realistic based on the electronic structure description of the NO complex (see below), which indicates that the unpaired electrons of the ligand have to be spin-paired because of the orbital overlap. In the case of the $S_{tot} = 1$ state, the unpaired electrons of the ligand are spin-paired (antiferromagnetic coupling); however, Fe^{III} is required to maintain an intermediate spin excited state ($S = {}^3/_2$). In the following, only calculations based on the $S_{tot} = 2$ state are considered.

Relevant geometric parameters of the geometry optimized model are listed in Table 6; for comparison, the corresponding parameters from the crystal structure of **1** and the {FeNO}[7] models optimized with BP86 + 10% HFX using LanL2DZ and 6-311G*/6-31G* are also included. The averaged Fe–L bond lengths (where L is any ligand except NO or O_2) are similar in the FeNO and FeO$_2$ complexes with either of the two basis sets considered. The major difference is in the geometry of the FeNO and FeO$_2$ units. It was established above that in the case of FeNO complexes the choice of the basis set shows significant effects on the N–O bond length (Tables 1 and 6). In contrast, in the FeO$_2$ complex, the selection of basis set not only strongly affects the O–O bond length, but also the Fe–O distance, the Fe–O–O angle, and the L-Fe–O–O dihedral angles (L being any of the remaining five Fe ligands). The geometric differences between the FeNO and FeO$_2$ units are greater in the models optimized with the LanL2DZ basis set than in those optimized with the mixed basis set. The Fe–L distances (L = N or O) differ by 0.25 Å in the models optimized with the former basis set, and by 0.15 Å when the latter is used. A similar observation is made for the Fe–N–O and Fe–O–O angles (LanL2DZ, 144° and 109°; 6-311G*/6-31G*, 148° and 130°, respectively; Table 6).[58] However, the same key structural differences are observed between the {FeNO}[7] and {FeO$_2$}[8] complexes optimized with the calibrated BP86 + 10% HFX functional, regardless of the choice of basis sets. The Fe–O$_2$ bond length is consistently longer than the Fe–NO bond length by ∼0.20 Å, and the Fe–O–O angle is also steeper than the Fe–N–O angle by ∼30° in both of the basis sets considered.

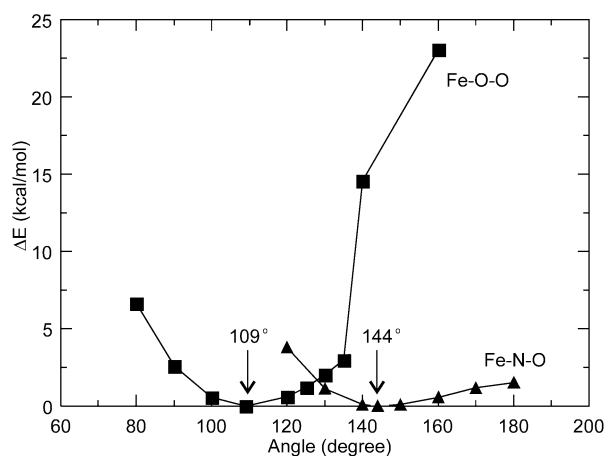To evaluate the angle dependence of the {FeNO}[7] and {FeO$_2$}[8] complexes, the potential energy surfaces (PES) of the

Figure 4. Dependence of the potential energy on the Fe–N–O and Fe–O–O angles. For {FeNO}[7], the PES is shallow, whereas for {FeO$_2$}[8] both oxidation and spin states change upon increasing the angle beyond a critical point.

Fe–N–O angle and Fe–O–O angle in the corresponding models optimized with the basis set LanL2DZ[59] were studied (Figure 4). Although {FeNO}[7] has a shallower potential energy well than {FeO$_2$},[8] varying the angles around the optimal values in the two complexes (∠FeNO = 144°, ∠FeO$_2$ = 109°) only raises the total energy by a maximum of ∼7 kcal/mol.[60] While σ interaction is optimal when the Fe–NO/O$_2$ angle is close to 90°, π interaction increases at wider angles. Thus, the angle preference of the two complexes is expected to reflect the relative contributions of σ and π interactions to bonding (vide infra).

Vibrational analysis was only conducted with the mixed basis set because it was shown above that a triple-ζ basis set is required to obtain good agreement between experimental and calculated stretch frequencies. For {FeO$_2$},[8] the calculated O–O stretch frequency is 1211 cm^{-1}, as compared to 1169 and 1609 cm^{-1} for O_2^- and O_2, respectively.

5. Energetics of NO/O$_2$ Binding in the Model Complex. Because insight into the relative energetics of NO and O_2 binding to the 5C model complex is necessary to develop an understanding of the different reactivities, NO was removed from **1** as a neutral molecule, and the resulting hypothetical, ferrous 5C complex was geometry optimized using BP86 + 10% HFX. Parallel studies were performed on the {FeO$_2$}[8] model. To evaluate the effects of the functional on the energetics, we expanded this analysis to include the functionals B3LYP and BP86 for comparison. Additionally, the effect of the basis sets (LanL2DZ and 6-311G*/6-31G*) was evaluated. Table 7 summarizes the results. It is important to emphasize that, regardless of the choice of functional or basis set, NO binding is far more exergonic than O_2 binding. The magnitude of the thermodynamic parameters varies considerably between different levels of theory (Table 7). The main source for these differences lies in the electronic energy ΔE. The enthalpy ΔH is in general very similar to ΔE, and the entropy term is only mildly affected by both functional and basis set. In the models

(57) The same energy order was observed for the model optimized with B3LYP and the mixed basis set, with the $S_{tot} = 2$ state favored by 7.9 and 11.5 kcal/mol as compared to the $S_{tot} = 1$ and $S_{tot} = 3$ states, respectively.

(58) It is interesting to note that the basic electronic structure description of both the NO and the O_2 models appears to be only mildly affected by the choice of the basis set used for the geometry optimization, as illustrated by the calculated Fe spin densities and charges for the {FeNO}[7] and {FeO$_2$}[8] models optimized with BP86 + 10% HFX and the basis sets LanL2DZ and 6-311G*/6-31G*, respectively (Table S3).

(59) The LanL2DZ optimized models were selected for further analysis because the differences in geometric parameters between {FeNO}[7] and {FeO$_2$}[8] are more pronounced than in the models optimized with the mixed basis set (Table 6).

(60) The rapid increase in the total energy of {FeO$_8$}[8] at ≥140° is due to a change in the ground-state electronic description.

Table 7. Energetics of NO and O₂ Binding to the Putative 5C Derivative of **1** with Various Functionals (BP86, BP86 + 10% HFX, and B3LYP) and Basis Sets (LanL2DZ and 6-311G*/6-31G*)

basis set	thermo-dynamics[a]	BP86		BP86 + 10% HFX		B3LYP	
		NO	O₂	NO	O₂	NO	O₂
LanL2DZ	ΔE	−42.80	−23.57	−29.87	−13.03	−20.31	−9.36
	ΔH	−43.39	−24.16	−30.46	−13.62	−20.90	−9.96
	$-T\Delta S^b$	12.82	12.22	11.99	11.76	12.71	12.33
	ΔG	−30.57	−11.94	−18.47	−1.86	−8.19	+2.37
6-311G*/	ΔE	−51.05	−26.93	−36.67	−15.69	−26.34	−13.08
6-31G*	ΔH	−51.64	−27.52	−37.26	−16.28	−26.93	−13.68
	$-T\Delta S^b$	13.37	12.77	12.38	11.94	10.48	12.27
	ΔG	−38.27	−14.75	−24.88	−4.34	−16.45	−1.41

[a] Energies in kcal/mol. [b] At 298 K.

optimized with BP86 + 10% HFX, NO binding is ∼20 kcal/mol more exothermic than O₂ binding.

It should be noted that the reaction with O₂ has a ΔG close to thermoneutral and would be expected to occur. This is in contrast to observations on the mononuclear non-heme iron enzyme 2,3-dihydroxybiphenyl 1,2-dioxygenase (DHBD), where both experimental and computational data have demonstrated a highly endothermic ΔG (≥20 kcal/mol) reaction.[61] Two possible factors can contribute to the lower reaction energy for the fictitious model complex. (1) The tri-dentate ligand *N,N′,N″*-trimethyl-1,4,7-triazacyclononane (Figure 1) constrains the ligand and may thus destabilize the Fe^II reactant. (2) The chemically different nature of the ligand sets may further add to the increased reactivity. To estimate the contribution of both ligand constraint and ligand set to the reactivity, modified model complexes were geometry optimized, using the methodology developed above. In one model, the constraint of the tri-dentate ligand set was removed by replacing the cyclononane by three amine groups. In the second model, the two azide groups (Figure 1) were replaced by hydroxides. Both substitutions lead to endothermic changes in the reaction energetics. Ligand constraint in the Fe^II[Me₃TACN] complex reduces ΔG of O₂ binding by ∼15 kcal/mol, and the ligand set reduces the free energy by another ∼3 kcal/mol. Hence, the calculated ΔG of the O₂ reaction increases from ∼ −4 kcal/mol (Table 7) to ∼ +15 kcal/mol in the unconstrained complex with less donating ligands, a value similar to that reported for the reaction of DHBD with O₂.[61]

Determining the origin of these dramatic differences in bonding energetics is essential to understanding the variations in reactivity. Because **1** is best described as an $S = {}^3/_2$ antiferromagnetically coupled Fe^III($S = {}^5/_2$)−NO⁻($S = 1$) complex,[5] and calculations presented in the next section show that {FeO₂}[8] can similarly be described as high-spin Fe^III ($S = {}^5/_2$) antiferromagnetically coupled to O₂⁻ ($S = {}^1/_2$), the bonding interaction was further considered in three steps. The five-coordinate ferrous complex is oxidized, NO/O₂ is reduced, and the oxidized complex and the reduced ligands are allowed to interact. These calculations were carried out using models optimized with the functional BP86 + 10% HFX and the mixed basis set 6-311G*/6-31G*. Each optimized model was subjected to a solvent calculation in ethanol, using $\epsilon = 24.55$ as the dielectric constant. Figure 5 shows an energy diagram including the individual steps in the reaction. Interestingly, the reduction
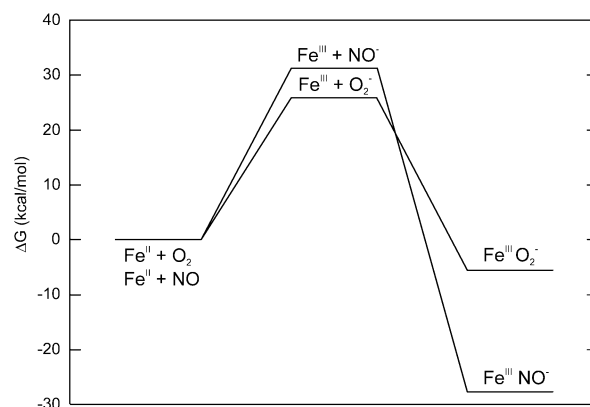

Figure 5. Energy profiles of the reactions between Fe^II and NO or O₂. The one-electron transfer step is highly endothermic, with the reduction of NO being less favorable. The driving force for the reaction with NO is the formation of strong Fe^III−NO⁻ bonds. In the reaction with O₂, Fe^III−O₂⁻ bonding interactions are also exothermic, however, to a much smaller extent. As a result, the O₂ binding reaction is less favorable.

of NO is more endothermic than that of O₂. Note that the redox part in Figure 5 comprises both the oxidation of the complex and the reduction of the ligand. Because the complex oxidation is the same for {FeNO}[7] and {FeO₂}[8], the difference in the energy profile is solely due to ligand reduction. Literature on the reduction potential of NO provides a wide spectrum of values, ranging from ∼ +0.4 to ∼ −0.8 V (referenced to the normal H electrode). Most recently, a detailed study by Fukuto, Houk, and co-workers, combining electrochemical measurements and ab initio calculations, has estimated the reduction potential of NO to be ∼ −0.8 V,[62] supporting a low driving force for NO reduction. For the reduction of O₂ to superoxide, a value of ∼ −0.3 V is generally accepted.[63,64]

Thus, NO is in fact harder to reduce than O₂. Factors that can contribute to this difference in potentials are orbital energy differences and differences in Coulomb and exchange interactions between electrons. The MO diagrams for NO and O₂ are shown in Figure 6. If one assumes that the Coulomb repulsions between electrons in two different π^* orbitals in NO and O₂ are similar, additional interactions between electrons arising from the reduction of NO and O₂ predict NO reduction ($J_{12} − K_{12}$) to be more favorable than O₂ reduction ($J_{12} + J_{11}$).[65] This is opposite to the experimental and theoretical results and suggests that the major contribution to the observed difference in the reduction potentials of NO and O₂ is associated with differences in orbital energies due to electronegativity differences, with the less electronegative nitrogen giving the major contribution to the $2\pi^*$ MO. This is qualitatively supported by photoelectron spectroscopy (PES) results, which show that O₂ is harder to ionize by ∼3 eV.[66]

Because the redox step in {FeNO}[7] is more endothermic than that in {FeO₂},[8] the main source for the increased reactivity of the 5C complex toward NO lies in the different bonding interaction of the reduced ligands with the oxidized complex.

(61) Davis, M. I.; Wasinger, E. C.; Decker, A.; Pau, M. Y. M.; Vaillancourt, F. H.; Bolin, J. T.; Eltis, L. D.; Hedman, B.; Hodgson, K. O.; Solomon, E. I. *J. Am. Chem. Soc.* **2003**, *125*, 11214−11227.
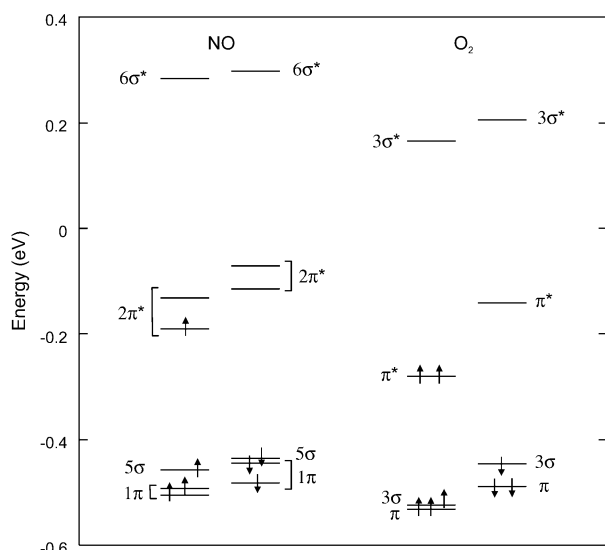
(62) Bartberger, M. D.; Liu, W.; Ford, E.; Miranda, K. M.; Switzer, C.; Fukuto, J. M.; Farmer, P. J.; Wink, D. A.; Houk, K. N. *Proc. Natl. Acad. Sci. U.S.A.* **2002**, *99*, 10959−10963.

(63) Wood, P. M. *Trends Biochem. Sci.* **1987**, *12*, 250−251.

(64) Sawyer, D. T. *Oxygen Chemistry*; Oxford University Press: New York, 1991.

(65) **1** and **2** represent the two π^* orbitals of NO and O₂ (π_{ip}^* and π_{op}^*).

(66) Rabalais, J. W. *Principles of Ultraviolet Photoelectron Spectroscopy*; John Wiley & Sons: New York, 1977.

Figure 6. Energy level diagrams for spin-unrestricted calculations of NO and O_2. The diatomics were optimized with BP86 + 10% HFX using the triple-ζ basis set 6-311G*.

Figure 5 shows that NO^- bonding is far more exothermic than O_2^- binding ($\Delta \approx 30$ kcal/mol), leading to a $\Delta G \approx -24$ kcal/mol (Table 7, BP86 + 10% HFX, 6-311G*/6-31G*). The origin of this key difference in bonding and its contribution to reactivity is considered below.

6. Electronic Structure Description. To gain insight into (i) the relative electronic structures of $\{FeNO\}^7$ and $\{FeO_2\}^8$ complexes, (ii) their relative energetics, and (iii) the role of the geometry on the bonding description, the MOs of several structures are compared. First, the optimized structures are analyzed (Figures 7–9), followed by a comparison of models with interchanged geometries; that is, the wave function for the $\{FeNO\}^7$ model was reconverged using the geometric parameters of the FeO_2 unit in the optimized $\{FeO_2\}^8$ model, and vice versa. The MOs and energy levels for these interchanged models are qualitatively similar to their corresponding optimized counterparts and are presented in Figures S2–S5.[67]

The MOs and energy level diagrams for the optimized $\{FeNO\}^7$ complex are shown in Figures 7 and 9, left, respectively. The five lowest-energy unoccupied MOs in the β manifold display predominantly iron 3d character. Because of spin polarization, their five occupied counterparts in the α manifold are greatly stabilized by ~6 eV (Figure 9, left). The two lowest unoccupied α MOs are predominantly NO $2\pi^*$ in character (MOs $\alpha87$ and $\alpha88$, Figure 7A and B), with small contributions from the metal ion (column 1 in Table 8). Here, we focus on these unoccupied MOs to evaluate the bonding contributions. While they are antibonding with respect to the Fe–NO interaction, they reflect the uncompensated occupied counterparts which give the major contribution to bonding. For $\{FeNO\}^7$, the unoccupied α NO $2\pi^*$ MOs have in-plane ($2\pi_{ip}^*$, MO $\alpha88$, Figure 7B) and out-of-plane ($2\pi_{op}^*$, MO $\alpha87$, Figure
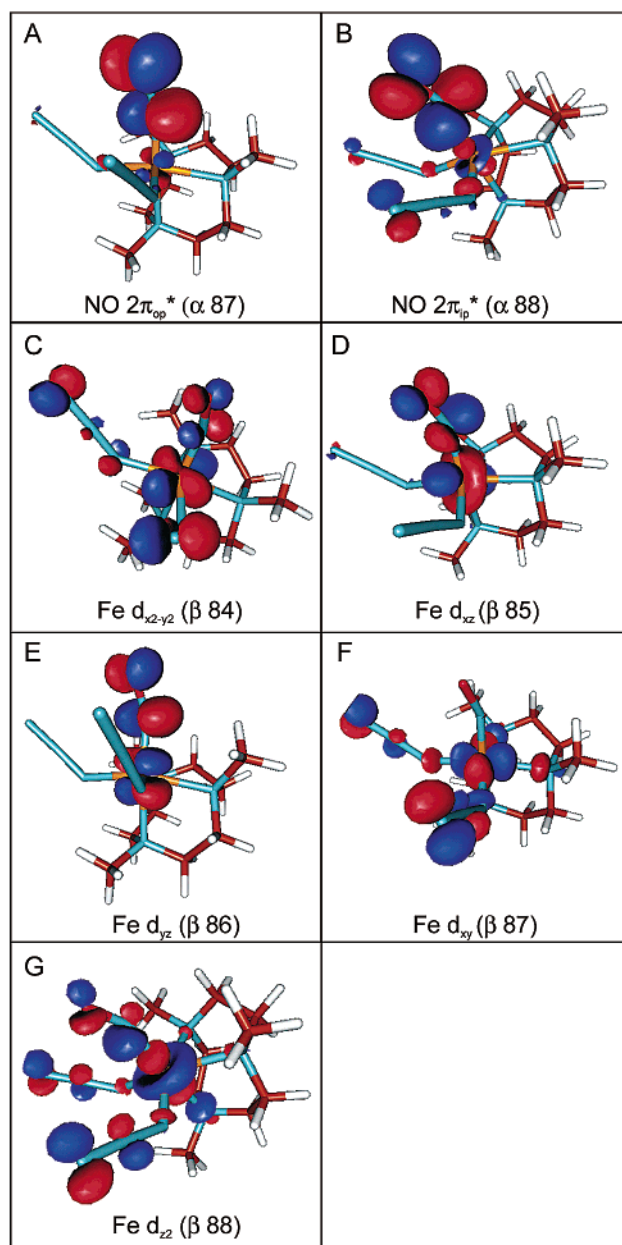
(67) The LanL2DZ optimized models were selected for this comparison because the differences in geometric parameter between $\{FeNO\}^7$ and $\{FeO_2\}^8$ are more pronounced than in the models optimized with the mixed basis set (Table 6). The electronic structure description does not depend on the choice between these two basis sets. It is noted that the NO and O_2 models optimized with the mixed basis set 6-311G*/6-31G* were compared in a similar manner and results analogous to the ones described here were obtained. For completion, the relevant MOs and energy levels are included in the Supporting Information (Figures S6–S12 and Table S4).
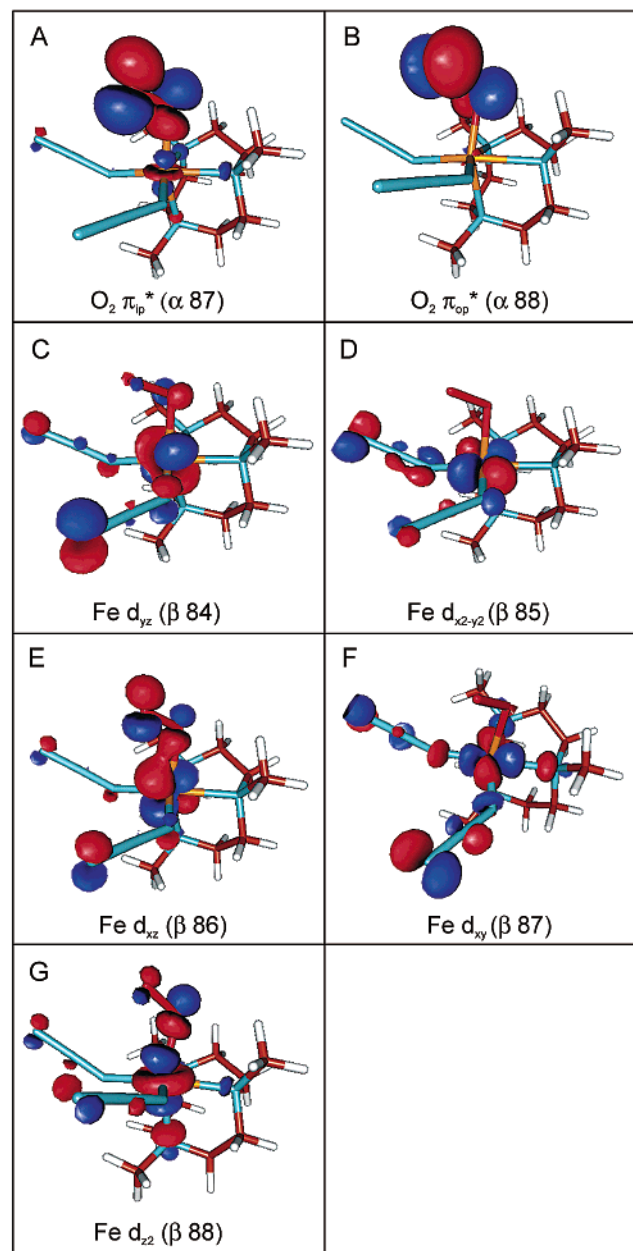
Figure 7. Molecular orbitals for $\{FeNO\}^7$ optimized with BP86 + 10% HFX and LanL2DZ. Only the two unoccupied α MOs with predominant $2\pi^*$ character and the five unoccupied, predominantly Fe 3d β MOs are shown.

7A) character; this is consistent with the presence of both σ and π bonding interactions between NO and the appropriate Fe 3d orbitals, the d_{xz} (8.5%) and d_{yz} (4.7%) MOs, respectively (column 1 in Table 8). Because of the short Fe–N bond, the $2\pi_{ip}^*$ is more destabilized than the $2\pi_{op}^*$ (Figure 9, left). Both σ and π interactions are also present in the five lowest energy unoccupied β MOs, with d_{xz} (MO $\beta85$, Figure 7D) and d_{z2} (MO $\beta88$, Figure 7G) having a σ antibonding interaction with NO $2\pi_{ip}^*$ (31.5%), and d_{yz} (MO $\beta86$, Figure 7E) has a π antibonding interaction with NO $2\pi_{op}^*$ (36.5%) (column 1 in Table 8). The MOs for the optimized $\{FeO_2\}^8$ complex are qualitatively similar and are presented in Figure 8. As compared to $\{FeNO\}^7$, the $\{FeO_2\}^8$ unit has one more α spin electron which resides in the O_2 π_{ip}^* MO (MO $\alpha87$, Figure 8A). As a result, essentially only one bonding interaction remains between Fe^{III} and O_2^-.

Figure 8. Molecular orbitals for {FeO$_2$}^{8} optimized with BP86 + 10% HFX and LanL2DZ. Only the two α MOs with predominant π^* character and the five unoccupied, predominantly Fe 3d β MOs are shown. Only one of the two π^* MOs is unoccupied.

Inspection of the unoccupied β MOs shows the presence of a σ bond comparable to that in the {FeNO}^{7} model (25.3% O$_2$ π_{ip}^* contribution (MOs β86 and β88, Figure 8E and G, column 2 in Table 8) as compared to 31.5% in the {FeNO}^{7} model (MOs β85 and β88, Figure 7D and G, column 1 in Table 8)) and the virtual lack of a π-bonding interaction, with only 4.2% O$_2$ π_{op}^* contribution (MO β84, Figure 8C, column 2 in Table 8) as compared to 36.5% in the {FeNO}^{7} model (MO β86, Figure 7E in Table 8). A measure of the relative bonding of the NO$^-$ and the O$_2^-$ with the Fe^{III} is given by the sum of the uncompensated σ and π contributions to both α and β manifolds, which amount to 81.2% and 30.0% for {FeNO}^{7} and {FeO$_2$}^{8}, respectively.

As mentioned above, the geometries of the {FeNO}^{7} and {FeO$_2$}^{8} units in the optimized FeNO and FeO$_2$ model com-

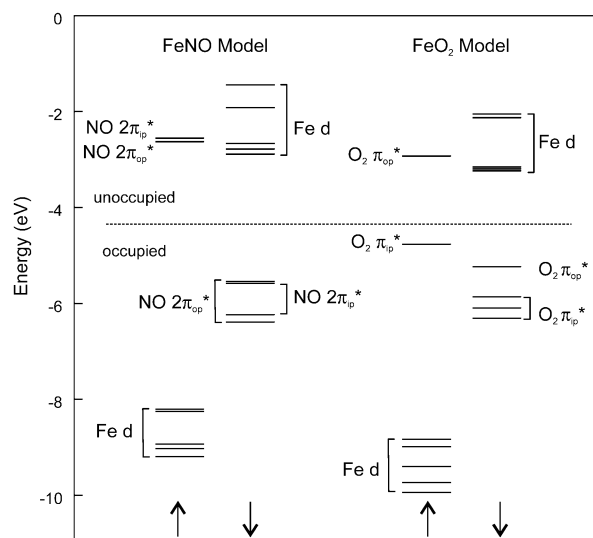**Figure 9.** Energy level diagrams for spin-unrestricted calculations of optimized {FeNO}^{7} and {FeO$_2$}^{8}. The arrows indicate the spin. The occupied Fe 3d MOs are greatly exchange stabilized. The most obvious difference between {FeNO}^{7} and {FeO$_2$}^{8} is the stabilization of one of the two α spin π^* MOs relative to the β spin Fe 3d MOs.

plexes differ significantly (Table 6). Independent of the choice of the basis set, the Fe−O bond is significantly longer than the Fe−N bond (LanL2DZ, 2.03 vs 1.78 Å; 6-311G*/6-31G*, 1.88 vs 1.72 Å), and the Fe−O−O angle is steeper than the Fe−N−O angle (LanL2DZ, 109° vs 144°; 6-311G*/6-31G*, 130° vs 148°). It is thus of interest to investigate the effect of geometry on the bonding description of the two complexes. Altering the geometry of the FeNO unit to that of the optimized FeO$_2$ unit (longer bond length and steeper angle) leads to the expected decrease in overlap (columns 1 and 3 in Table 8; Figure S2) and a destabilization of π_{op}^* relative to π_{ip}^* (Figure S4). The uncompensated covalent mixing (vide supra) of the {FeNO}^{7} complex reduces from 81.2% to 48.7%; however, both the σ and the π bonding interactions are still present. The bonding interaction is still stronger in this {FeNO}^{7} complex (48.7%) relative to the {FeO$_2$}^{8} complex (30.0%) in the same geometry (columns 2 and 3 in Table 8). Analogously, altering the geometry of the {FeO$_2$}^{8} complex to that of the optimized {FeNO}^{7} structure (shorter bond length and wider angle) results in an increase in orbital overlap (columns 2 and 4 in Table 8; Figure S3). Because of the shorter Fe−O bond, the π_{ip}^* MO is destabilized and therefore higher in energy than the π_{op}^* MO (Figure S5). Thus, in contrast to the geometry optimized {FeO$_2$}^{8} model in Figure 8, the extra electron in the α manifold now resides in the π_{op}^* orbital. At this contracted geometry, {FeO$_2$}^{8} has a stronger π bond (32.1% vs 4.7%), while the σ interaction (26.4%) has not changed greatly from that in the optimized structure (25.8%). Although the uncompensated covalent mixing in this {FeO$_2$}^{8} complex increases from 30.0% to 58.5%, the bonding interaction is still considerably weaker than that in the optimized {FeNO}^{7} model (81.2% vs 58.5%, columns 1 and 4 in Table 8), consistent with the above correlation for the {FeO$_2$}^{8} geometry.

Discussion

Studies on mononuclear non-heme iron enzymes, such as the extradiol dioxygenases, indicate that the resting 5C ferrous active

Table 8. Comparison of MO Coefficients among Various FeNO and FeO$_2$ Models with the LanL2DZ Basis Set

	FeNO optimized model				FeO$_2$ optimized model				FeNO model with FeO$_2$ optimized geometry				FeO$_2$ model with FeNO optimized geometry			
	label	occup	%3d	%NO	label	occup	%3d	%O$_2$	label	occup	%3d	%NO	label	occup	%3d	%O$_2$
α88	$2\pi_{ip}^*$	0	8.5	79.6	π_{op}^*	0	0.5	97.4	$2\pi_{op}^*$	0	1.3	94.4	π_{ip}^*	0	5.8	85.4
α87	$2\pi_{op}^*$	0	4.7	89.4	π_{ip}^*	1	6.1	84.3	$2\pi_{ip}^*$	0	4.2	84.6	π_{op}^*	1	9.3	23.4
α86													π_{op}^*	1	4.5	54.6
α84													π_{op}^*	1	2.9	14.1
β88	z^2	0	57.7	12.3	z^2	0	68	11.9	z^2	0	64	13.8	z^2	0	64.2	11.5
β87	xy	0	63.5	0.7	xy	0	64	0.6	xy	0	62.8	1.5	xy	0	63	1.5
β86	yz	0	60.2	36.5	xz	0	74.3	13.4	xz	0	79.8	6.5	yz	0	63.2	32.1
β85	xz	0	73.7	19.2	$x^2 - y^2$	0	76.7	0.5	$x^2 - y^2$	0	76.2	0.8	xz	0	85	9.1
β84	$x^2 - y^2$	0	71.2	8.2	yz	0	76.9	4.2	yz	0	63.2	22.9	$x^2 - y^2$	0	71.7	2.6

site reacts only slowly with oxygen[68] but readily with NO.[2] A recent study[61] on the resting 5C form of DHBD has shown that the one-electron transfer from Fe^{II} to O$_2$ is highly unfavorable, and although the bond formation of the resultant Fe^{III} with O$_2^-$ is exothermic, it does not provide enough stabilization to drive the reaction.[69] The difference in reactivity of resting mononuclear non-heme iron enzymes toward NO and O$_2$ to form the corresponding Fe^{III}−NO$^-$ and Fe^{III}−O$_2^-$ complexes had generally been considered to be attributed to the difference in their reduction potentials. However, a recent study by Fukuto, Houk, and co-workers on the reduction potential of the NO/NO$^-$ couple using a combination of experimental and computational methods indicated that NO is in fact more difficult to reduce than O$_2$.[62] Hence, the main contribution to the observed differences in reactivity of Fe^{II} toward NO and O$_2$ should be the difference in the strength of the resultant Fe^{III}−NO$^-$ and Fe^{III}−O$_2^-$ bonds. In this study, spin-unrestricted DFT calculations with an experimentally optimized level of theory were used to analyze the relative reactivities of the 5C Fe^{II} derivative of **1** toward NO and O$_2$ (Figure 5). Similar to the resting form of DHBD, the one-electron transfers from Fe^{II} to NO and O$_2$ are highly unfavorable. However, the more negative free energy of the reaction between Fe^{III} and NO$^-$ as compared to that between Fe^{III} and O$_2^-$ demonstrates that the difference in bonding interaction of NO$^-$ and O$_2^-$ with Fe^{III} is the origin of the large difference in reactivity (Figure 5). NO$^-$ forms a much stronger bond with Fe^{III} than O$_2^-$, and this is reflected in the different electronic structures of the {FeNO}^{7} and {FeO$_2$}^{8} complexes (Figures 7−9).

Experimental and theoretical data provided strong evidence for the description of the electronic structure of **1** as an $S = \frac{3}{2}$ antiferromagnetically coupled Fe$^{III}(S = \frac{5}{2})$−NO$^-(S = 1)$ complex.[5] The observation of five unoccupied β MOs with predominant Fe 3d character, and the presence of two unoccupied NO $2\pi^*$ MOs in the α manifold of the geometry optimized {FeNO}^{7} (Figure 7), agree with our previous study and are consistent with this bonding description of the {FeNO}^{7} unit. The strong exchange coupling requires considerable orbital overlap between the metal ion and NO$^-$, implying strong donor bonding interactions from the NO$^-$ ligand. A comparison between NO$^-$ and the geometry optimized {FeNO}^{7} complex shows that the experimental (1346 vs 1712 cm^{-1}) and calculated (1420 vs 1758 cm^{-1}) N−O stretch frequencies are significantly

higher in the {FeNO}^{7} model. Inspection of the unoccupied MOs in the β manifold (i.e., Fe^{III}) shows a large contribution from the $2\pi^*$ orbitals of the NO$^-$ ligand. Because these MOs are antibonding with respect to the ligand, removal of charge strengthens the intraligand bond, resulting in an increased N−O stretch frequency.

Geometry optimization of the putative FeO$_2$ derivative of **1** shows an electronic structure analogous to that of the {FeNO}^{7} model. The extra electron in {FeO$_2$}^{8} resides in one of the two α spin π^* MOs, leading to an electronic description of high-spin Fe^{III} ($S = \frac{5}{2}$) antiferromagnetically coupled to O$_2^-$ ($S = \frac{1}{2}$), giving $S_{tot} = 2$. Because this extra electron occupies an Fe^{III}−O$_2^-$ antibonding orbital, the strength of the Fe^{III}−O$_2^-$ bond is weaker than the Fe^{III}−NO$^-$ bond. This is consistent with the longer Fe−O$_2$ bond (LanL2DZ, 2.03 vs 1.78 Å; 6-311G*/6-31G*, 1.88 vs 1.72 Å) in the geometry optimized FeO$_2$ model in comparison to the FeNO model (Table 6). The calculated O−O stretch frequency in the {FeO$_2$}^{8} complex (1211 cm^{-1}) is only moderately higher than the calculated value of the free O$_2^-$ anion (1169 cm^{-1}), indicating that limited electron density has been donated from the antibonding orbital of the O$_2^-$ ligand. This observation agrees with the bonding energetics and the weaker Fe^{III}−O$_2^-$ bond.

The differences in geometric and electronic structures between {FeNO}^{7} and {FeO$_2$}^{8} arise from the extra electron in the latter system. Both σ and π bonding interactions are observed in the {FeNO}^{7} complex, with 8.5% σ and 4.7% π in the α manifold and 31.5% σ and 36.5% π in the β manifold. In the case of {FeO$_2$}^{8}, the extra electron resides in the α O$_2^-$ $2\pi_{ip}^*$ orbital, which σ interacts with the Fe 3d orbitals. This occupation in the antibonding orbitals eliminates the σ bonding interaction, leaving only a weak π interaction of 0.5% on the α manifold. While both σ and π interactions are present in the β manifold, the bond is essentially of σ character (25.3% σ and 0.6% π), although spin-restricted molecular orbital theory would predict the single bond to be of π type between the half occupied π_{op}^* and the metal ion. In the spin-unrestricted description, electron repulsion between the α and β spins in the doubly occupied in-plane MO raises its energy above the singly occupied out-of-plane MO, leading to considerable mixing between the π_{ip}^* and the Fe 3d MOs (Figure 8). The difference in Fe−NO and Fe−O$_2$ bond lengths and Fe−N−O and Fe−O−O angles reflects these different bonding descriptions. The longer Fe−O$_2$ bond is consistent with a much weaker interaction between Fe^{III} and O$_2^-$, and the steeper Fe−O−O angle is consistent with a bonding interaction dominated by σ overlap. The presence of an additional electron reduces the bonding from 1 σ plus 1 strong

(68) Vaillancourt, F. H.; Labbe, G.; Drouin, N. M.; Fortin, P. D.; Eltis, L. D. *J. Biol. Chem.* **2002**, *277*, 2019−2027.
(69) It should be noted that when substrate binds to Fe^{II}, the O$_2$ reactivity greatly increases.[2] In the ES complex, substrate contains high-lying occupied orbitals available for transfer of an additional electron, allowing the favorable two-electron reduction of O$_2$ to O$_2^{2-}$.[61]

π bond in {FeNO}[7] to only 1 σ bond in {FeO₂}.[8] It is this difference in bonding to the Fe^{III} that results in the greater stability of the $Fe^{III}-NO^-$ bond in the {FeNO}[7] complex, leading to a thermodynamically more favorable reaction between Fe^{II} and NO (Figure 5).

In summary, our studies applied an experimentally optimized DFT approach to gain insight into the electronic structure and reactivity of {FeNO}[7] and {FeO₂}[8] complexes. Using the crystal structure of **1** as a marker, we found that BP86 + 10% HFX is an optimal functional for these investigations. Comparison of calculated parameters for the fully optimized model to experimental vibrational and excited-state data supports this approach. The energetics of NO and O_2 binding were then analyzed. The choice of the basis set, which mainly affects the geometry of the FeNO and FeO₂ units, has a modest effect on the thermodynamic parameters of NO and O_2 binding. Using this experimentally calibrated DFT approach, we compared the electronic structure and reactivity of **1** to that of the analogous {FeO₂}[8] hypothetical complex. The reaction with NO, involving charge transfer to give a description of Fe^{III} ($S = \frac{5}{2}$) antiferromagnetically coupled to NO^- ($S = 1$), is greatly favored due to stronger bonding interactions, involving both σ and π bonds, between NO^- and Fe^{III}. In contrast, the FeO₂ model, which has a similar electronic description (Fe^{III} ($S = \frac{5}{2}$) antiferromagnetically coupled to O_2^- ($S = \frac{1}{2}$)), has only one bonding interaction; the weaker bond between Fe^{III} and O_2^- results in less charge donation from O_2^- to Fe^{III}, a longer $Fe^{III}-O_2^-$ bond, and a weakened $O-O^-$ bond. Because NO is often used as an analogue to study potential FeO₂ intermediates in protein-catalyzed reactions, this study provides a basis for relating the electronic structures of NO complexes to those of the corresponding O_2 complexes and provides insight into their relative reactivities. We are now in the process of applying this {FeNO}[7] → {FeO₂}[8] approach to a variety of non-heme iron enzymes.

Supporting Information Available: Table of transition energies (ES1−ES3) obtained from ADF2001 ΔSCF-DFT calculations with BP86 and BLYP at varied Z_{eff} on models optimized with BP86 + 10% HFX and B3LYP using 6-311G*/6-31G* as the basis set (Table S1); table of Fe and NO spin densities obtained from Gaussian optimized models (BP86 + 10% HFX and B3LYP with 6-311G*/6-31G*) and those obtained from ΔSCF-DFT with BP86 and BLYP at optimal $Z_{eff} = 25.60$ (Table S2); table of Fe spin densities and charges for BP86 and 10% HFX optimized models (Table S3); overlay of spectroscopic data and TDDFT calculations on complex **1** optimized using B3LYP and 6-311G*/6-31G* (Figure S1); molecular orbitals and energy level diagrams for LanL2DZ calculations of {FeNO}[7] in the optimized {FeO₂}[8] geometry and vice versa (Figures S2−S5); molecular orbitals, energy level diagrams, and table of MO coefficients for all 6-311G*/6-31G* calculations of various {FeNO}[7] and {FeO₂}[8] models (Figures S6−S12 and Table S4) (PDF). This material is available free of charge via the Internet at http://pubs.acs.org.

JA036715U